Stochastic noise sources for broadband computational aeroacoustics applied to a simplified vehicle underbody geometry

Philipp Uhl[1], Alexander Schell[1], Roland Ewert[2], Jan Delfs[2]

[1] *Mercedes-Benz AG, 71063 Sindelfingen, corresponding author: philipp.uhl@mercedes-benz.com*

[2] *Institute of Aerodynamics and Flow Technology, DLR Braunschweig, 38108 Braunschweig*

Introduction

The need for fast yet accurate and reliable simulation techniques predicting the aeroacoustics of industrial test cases increases. Even though computational resources grow and the access to high-performance computing centers gets affordable, highly resolved simulations for computational aeroacoustics are still extremely expensive. For broadband noise phenomena, especially stochastic noise source methods have proven their prediction capabilities over the last years. In this work, two stochastic noise source methods, the Fast Random Particle Mesh (FRPM) method and the Forced Model Advection Equation (FAME), are juxtaposed in their prediction quality of nearfield aeroacoustic phenomena. The latter method FAME is based on the isotropic source realization approach FRPM and extends it by an anisotropic realization in the two-point turbulence statistics. Both methods are compared at two different underbody geometries of a simplified vehicle with a frequency range of interest of 40 Hz − 800 Hz. The extension with anisotropic length scales is expected to behave more robust by theoretically increasing the complexity of the modelling assumptions.

Theory and numerical methods

The basis for the stochastic noise source methods FRPM and FAME is a steady RANS computation. In a predefined region of interest, the velocity field u_i and turbulent data (turbulent kinetic energy k and turbulent length scale l_s) are extracted and taken for FRPM and FAME to realize turbulent velocity fluctuations u_i'. FRPM synthesizes velocity fluctuations which are isotropic in amplitude and isotropic in length scale by isotropically filtering a spatially varying white noise field with an isotropic filter width. FAME however distorts the isotropically filtered fluctuating components with the additional Forced Model Advection Equation, a transport equation which realizes anisotropy in length scales. Further information on FRPM can be found in Ewert [1] and on FAME in Ewert [2]. Both methods were already investigated in Liberson et al. [3, 4] for aeroacoustic spectra. In Reiche et al. [5], the realized anisotropic velocity fluctuations are studied more in detail.

Since the direct evaluation of the pressure spectra in the acoustic nearfield is necessary, a hydrodynamic/acoustic splitting approach is employed. The synthesized velocity fluctuations u_i' are converted to turbulent, hydrodynamic pressure fluctuations p_h' with a Poisson equation and further processed to acoustic pressure fluctuations p_a' with a Perturbed Convective Wave Equation [6]. This workflow $u_i' \rightarrow p_h' \rightarrow p_a'$ was already successfully applied to multiple test cases with generic and realistic geometries in Uhl et al. [7, 8]. The numerical simulations are processed in Simcenter Star-CCM+, the FRPM and FAME realizations are done with a software module from DLR.

Test case and computational setup

The simplified vehicle geometry used in this work with two different variations of the underbody, a flat and a more detailed underbody, was developed in Zhang et al. [9]. Both geometries are shown in figure 1 with relevant evaluation points P7, P14 and P11.

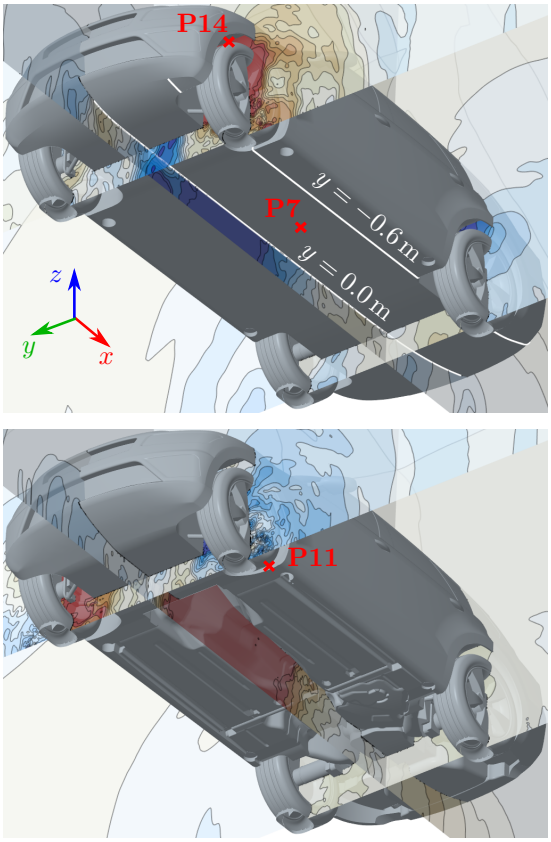

Figure 1: Schematic view on geometries of underbody with acoustic pressure p_a' (colorbar limits $p_a' \pm 5$ dB) on isosurfaces $y = 0.0$ m and $x = \{0.0, 2.8\}$m; top: flat underbody with evaluation points P7 and P14 and isolines at $y = \{0.0, -0.6\}$m; bottom: detailed underbody with evaluation point P11

Furthermore, for the flat variant, the two white lines indicate lateral positions in y for evaluating the mean pressure distribution in the results section. The inflow velocity amounts to $U_0 = 140$ km/h. The stochastic methods use an isotropic grid size of 8 mm, the LES decreases the

cell size to the walls and resolves the viscous sublayer. The time step equals $4 \cdot 10^{-5}$ s ensuring 31 points per wavelength for the upper frequency limit. Due to computational reasons, the noise sources are only realized on a block starting in front of the front wheels and ending in front of the rear wheels. Additionally, for the flat underbody variant, the symmetry of the test case is used to only take one front wheel into account. The detailed underbody has a symmetrical source weighting function in y capturing the entire lateral dimension of the vehicle.

Results

This section is organized as follows: first, results at the flat underbody geometry with the isotropic source realization method based on the FRPM approach are shown. With a length scale investigation of the LES showing evidence on length scale anisotropy, the usage of the anisotropic source realization method based on the FAME is motivated. The results are revisited with the anisotropic method and compared to the isotropic approach. With a transfer to the detailed underbody geometry, the methods are juxtaposed at a more realistic test case. The RANS model used for providing turbulent input data is the k-ε Lag Elliptic Blending model whereas for the subgrid scales of the LES, the Wall-Adapting Local Eddy Viscosity model is used.

Isotropic source realization results

Based on the previously described setup and models, results with velocity fluctuations using the isotropic FRPM approach can be computed. Besides the velocity and turbulent kinetic energy field which are a direct solver output of the RANS model, the turbulent length scale l_s needs to be prescribed. The length scale can be derived to $l_s = c_l k^{3/2}/\varepsilon$ with $c_l = 0.54$. Due to the empiricism in the calibration constant c_l, an additional length scale factor l_f is introduced leading to $l_s' = l_f l_s$ which globally modifies the length scale. A sensitivity study on this parameter l_f can be seen in figure 2 showing the acoustic pressure spectrum at P14 in the wheelhouse.

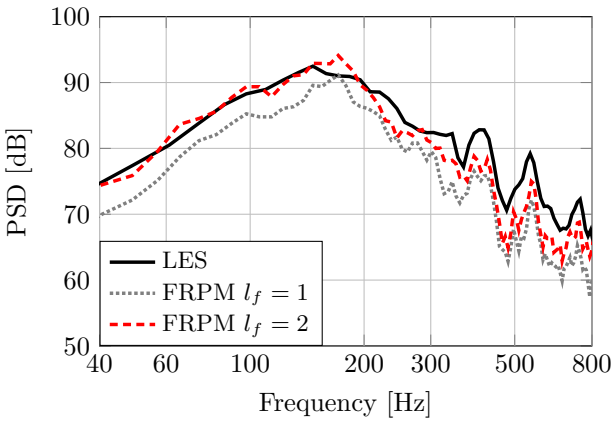

Figure 2: FRPM results with length scale sensitivity study of acoustic pressure p_a' to LES at P14 in wheelhouse

As can be seen a global increase of the length scale shifts the overall spectrum up. This can be traced back to the target energy distributions being input for the realization of a turbulent model spectrum. Whereas for lower frequencies, FRPM can reproduce the overall acoustics, for higher frequencies, an underestimation is computed. As can be shown later, this frequency range is influenced by anisotropic structures. The modes at > 400 Hz are geometrically induced and can be therefore predicted even though a broadband method like FRPM is used to excite the acoustics.

Motivation for anisotropic approach

To analyse the degree of anisotropy in the two-point turbulence statistics, the length scales from the LES are evaluated along lines aligned with the coordinate system. This can be done from two-point spatial correlations via

$$\Lambda_{ij}^{n}(\mathbf{x}) = \int_0^\infty \frac{\langle u_i(\mathbf{x},t) \cdot u_j(\mathbf{x}+\mathbf{r_n},t)\rangle}{\sqrt{\langle u_i^2(\mathbf{x})\rangle \langle u_j^2(\mathbf{x}+\mathbf{r_n})\rangle}} \mathbf{dr_n} \qquad (1)$$

with $\Lambda_{ij}^{n}(\mathbf{x})$ as the turbulent length scale at point $\mathbf{x}$ in direction n with distance $\mathbf{r_n}$ in between the two evaluated points based on the velocity components u_i and u_j. Anisotropic deformation of turbulent structures is especially caused by mean flow distortions, e.g. shear layers or strong pressure gradients. Insights into the mean flow distribution and anisotropic structures are given in figure 3 showing the mean pressure coefficient distribution $c_p = (\overline{p} - p_{ref})/(\rho/2U_0^2)$ of the LES at the two lateral lines $y = \{0.0, -0.6\}$m of figure 1. Furthermore, the turbulent length scales Λ_{ii}^{i} are evaluated at a point in close vicinity of the front wheelhouse. Later, it is shown that this region is dominant for acoustic contribution.

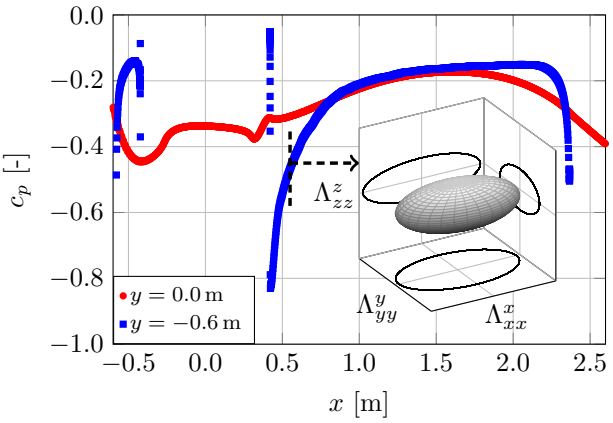

Figure 3: Pressure coefficient c_p of LES at two lateral locations (see figure 1) with subplot showing anisotropic length scales at point $(0.55, -0.6, 0.18)$m as semi-axes of ellipsoid (axis limits $\Lambda_{ii}^{i} = \pm 0.05$ m)

It can be seen that especially near the wheelhouses in a range of $x = 0.45$ m-0.7 m, a low pressure peak with subsequent strong adverse pressure gradient is present. The length scales reveal elongated structures with stretching in streamwise direction and approximately universal behaviour in lateral and wall-normal direction.

Anisotropic source realization results

Knowing this, the stochastic method based on FAME realizing anisotropic sources is employed. The identical point P14 in the wheelhouse as in figure 2 is chosen and revisited in figure 4 to compare the acoustic pressure p_a'.

In the filtering operation and advection equation, a turbulent time scale $t_s = k/\varepsilon$ is involved. Similarly to the empirical adaptation of the length scale l_s, the time scale is modified globally to $t_s' = t_f t_s$. With increasing t_f, not only the decay of the fluctuations is slowed down, but also the realized anisotropy is enhanced.

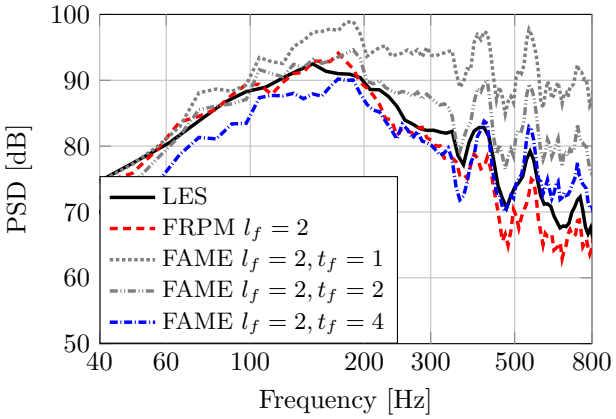

Figure 4: FAME results with anisotropy sensibility study of acoustic pressure p_a' to LES at P14 in wheelhouse

Choosing a too small time scale introduces high frequency noise due to an exaggerated temporal decay in the random values. Increasing this value to $t_f = 4$ especially improves the high frequency components that are underestimated with the isotropic FRPM method. However, the low frequency components are deteriorated slightly. This difference in the acoustic pressure is assumed to happen due to the introduced transport equation which requires temporal and spatial evolution to develop the distorted fluctuations. Lower amplitudes in the acoustic source can be observed at upstream located positions in front of the wheel. Especially for the interior noise up to 800 Hz, the entire perturbation pressure as sum of the hydrodynamic pressure p_h' and the acoustic pressure p_a' is relevant. Thus, both pressure variables must be in close agreement to the reference data in order to reliably use a stochastic method to replace LES. An improvement in the hydrodynamic pressure p_h' in the wake of the wheel and on the flat underbody is shown in figure 5.

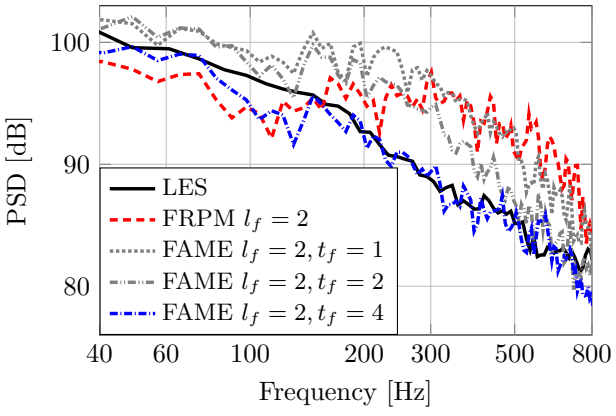

Figure 5: FAME results with anisotropy sensibility study of hydrodynamic pressure p_h' to LES at P7 on flat underbody

Even though the point P7 is only located on the flat underbody in the wake of the wheel, it is subject to the elongated structures caused by the acceleration in the channel-like underbody flow. The anisotropic method FAME with $t_f = 4$ delivers good results in the hydrodynamic surface pressure whereas FRPM overpredicts from 200 Hz due to incorrect characteristics of the realized vortices imprinting pressure fluctuations on the wall.

Transfer to more realistic geometry

The improvement of the overall agreement of the surface pressure data to the reference simulations by capturing certain anisotropic effects raises the idea to further investigate the generalizability of the stochastic method. A more detailed underbody geometry is therefore employed which is also shown in figure 1. The more realistic geometry introduces further aeroacoustic sources. Whereas for the flat underbody, mainly the wheelhouse edges contribute to the acoustic pressure, for the detailed underbody the edges become more complex, the flow more three-dimensional and the detaching shear layer additionally excites the cavity normally hosting the transmission. For a point P11, see figure 1, in close vicinity of the wheelhouse edges, the acoustic spectrum is shown in figure 6 for both stochastic methods with the previously found parameters compared to the reference LES.

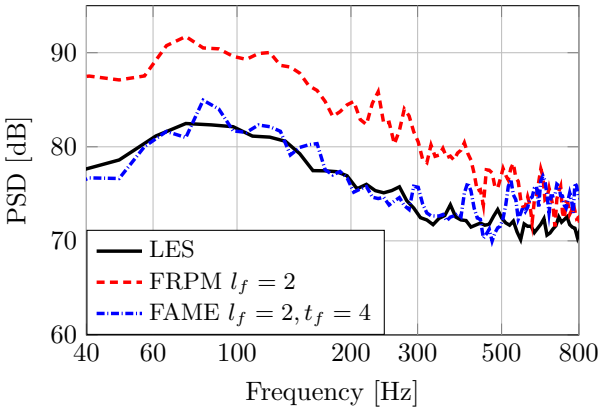

Figure 6: FRPM vs. FAME results of acoustic pressure p_a' to LES at P11 for detailed underbody geometry

The superiority of the more complex FAME method can be clearly seen. To visualize the relevant aeroacoustic source locations, a method shown in Delfs and Lebedev [10] is used. Solely based on the hydrodynamic pressure field p_h', a diffraction filter is derived which marks geometrical features that diffract the pressure field efficiently by introducing a reduced surface pressure p_s. This surface pressure is shown for the three used methods in the following figure for 100 Hz. The method has the advantage of relying only on vortical, i.e. turbulent, length scales $\lambda_w \simeq \lambda Ma$ with $\lambda = c/f$ the acoustic wave length and $Ma = U_0/c$ the Mach number with c as the speed of sound. At 100 Hz and for $U_0 = 140$ km/h, this amounts to the acoustic wavelength $\lambda = 3.4$ m and the vortical wavelength $\lambda = 0.389$ m. Methods relying on the acoustic surface data would not show a picture as precise and sharp as figure 7.

The main features of the aeroacoustic surface sources are in very close agreement between FAME and the ref-

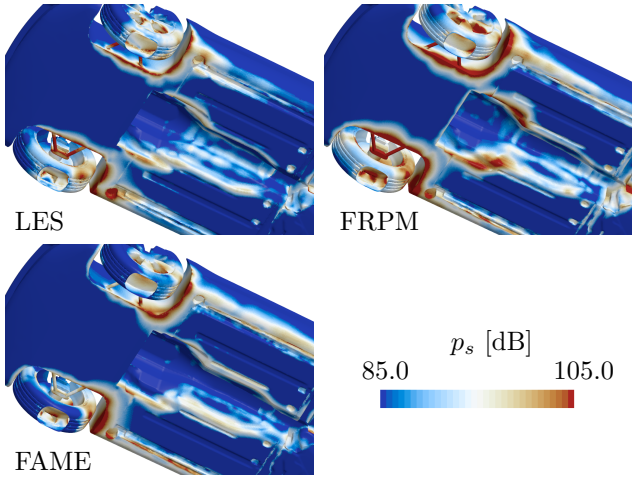

Figure 7: Reduced surface pressure p_s at 100 Hz for three methods referring to figure 6

erence LES whereas FRPM overestimates relevant areas at the wheelhouse edges or near the cardan tunnel. These edges as well as strong shear layer gradients in between the accelerated underbody flow and the calm recirculation cavity of the cardan tunnel are the source for anisotropy and different hydrodynamic/acoustic characteristics which are not accurately captured with the isotropic source realization approach FRPM.

Computational effort

The computational resources needed by the three different approaches, the reference LES, RANS-based FRPM and RANS-based FAME, consist of the following steps. The reference workflow starts with a RANS to initialize the flow field, then precomputes with a coarse time step a first unsteady field and finalizes the computation with the fine time step needed for an adequate flow and acoustics simulation. The stochastic methods use a similar workflow. They first start with a RANS simulation to compute the input data, then second either the FRPM method or the FAME approach is used to realize turbulent velocity fluctuations, and third the fluctuations are converted with the Poisson equation and propagated with the PCWE. The additional advection equation within the FAME approach only minorly increases the realization time. The largest part of this stochastic noise source methods workflow is the conversion and propagation in the third step. Comparing the stochastic workflow with the reference workflow, a computational speed-up of factor 8 can be observed, i.e. both stochastic workflows only need approx. 13% of what the reference LES needs.

Conclusion

Two stochastic noise source methods are compared to a reference LES at simplified vehicle underbody geometries with a focus on frequencies up to 800 Hz. The two stochastic methods differ in the realization of two-point turbulence statistics. The first method, FRPM, computes isotropic length scales, whereas the second method, FAME, can model distorted turbulent structures by taking an additional advection equation into account. Converting the realized velocity fluctuations to hydrodynamic pressure fluctuations by using a Poisson equation and propagating these with the PCWE to acoustic pressure fluctuations shows the superiority of the more complex, anisotropic source realization method. Already at a flat underbody geometry, significant improvements can be achieved by modelling elongated turbulent structures. At a more realistic underbody geometry, the more complex method shows its higher generalizability due to more complex assumptions in the modelling procedure.

References

[1] Ewert, R.: RPM - the fast Random Particle-Mesh method to realize unsteady turbulent sound sources and velocity fields for CAA applications. AIAA 2007-3506, 2007

[2] Ewert, R.: Canonical Stochastic Realization of Turbulent Sound Sources via Forced Linear Advection-Diffusion-Dissipation Equation. AIAA 2016-2965, 2016

[3] Liberson, L. and Lummer, M. and Mößner, M. and Reiche, N. and Ewert, R. and Delfs, J.: Zur Längenskalenanisotropie in der Modellierung des Kopfspaltgeräusches von Axialventilatoren. Fortschritte der Akustik - DAGA 2020

[4] Liberson, L. and Reiche, N. and Ewert, R. and Delfs, J.: Einsatz erweiterter Modellierung von Längenskalenanisotropie zur Vorhersage des Kopfspaltgeräusches von Axialventilatoren. Fortschritte der Akustik - DAGA 2021

[5] Reiche, N. and Ewert, R. and Delfs, J.: Aeroakustische Quelle aus anisotroper Turbulenz mittels synthetisch angeregter Turbulenztransportgleichung. Fortschritte der Akustik - DAGA 2021

[6] Piepiorka, J. and von Estorff, O.: Numerical investigation of hydrodynamic / acoustic splitting methods in finite volumes including rotating domains. Proceedings of the 23rd International Congress on Acoustics, 1827-1834, 2019

[7] Uhl, P. and Schell, A. and Ewert, R. and Delfs, J.: Validation of the Fast Random Particle-Mesh Method for Broadband CAA of a Forward-Facing Step and its prediction sensitivity for geometrical modifications. AIAA 2023-3499, 2023

[8] Uhl, P. and Schell, A. and Ewert, R. and Delfs, J.: Stochastic Noise Sources for Computational Aeroacoustics of a Vehicle Side Mirror. SAE Int. J. Passeng. Veh. Syst., 2024

[9] Zhang, C. and Tanneberger, M. and Kuthada, T. and Wittmeier, F. and Wiedemann, J. and Nies, J.: Introduction of the AeroSUV-A New Generic SUV Model for Aerodynamic Research. WCX SAE World Congress Experience, 2019

[10] Delfs, J. and Lebedev, V.: Ermittlung von aerodynamischen Schallquellen auf turbulent überströmten Oberflächen. Fortschritte der Akustik - DAGA 2024